ORGANOMETALLICS

Tutorial

Cite This: Organometallics 2018, 37, 3228–3239

pubs.acs.org/Organometallics

Pitfalls in Computational Modeling of Chemical Reactions and How To Avoid Them

Ho Ryu,[†,‡] Jiyong Park,[†,‡] Hong Ki Kim,[†,‡] Ji Young Park,[†,‡] Seoung-Tae Kim,[†,‡] and Mu-Hyun Baik*[,†,‡]

[†]Department of Chemistry, Korea Advanced Institute of Science and Technology (KAIST), Daejeon 34141, Republic of Korea

[‡]Center for Catalytic Hydrocarbon Functionalizations, Institute for Basic Science (IBS), Daejeon 34141, Republic of Korea

Supporting Information

ABSTRACT: Quantum chemical molecular modeling has become a standard tool in organometallic chemistry. In particular, density functional theory calculations are now indispensable for investigating the mechanism of even complex reactions and deliver precise energies of intermediates and transition states. Because software packages have become user-friendly and are widely available, even nonexperts can now produce high-quality computer models. In this tutorial, we highlight nontrivial mistakes, misconceptions, and misinterpretations often encountered when producing models of a chemical reaction that can lead to wrong conclusions. The reasons for these errors are conceptually explained in simple terms, and remedies are offered.

■ INTRODUCTION

Quantum chemical molecular modeling has become an indispensable tool for understanding the electronic structure and bonding of organometallic complexes. User-friendly software packages that are distributed conveniently and professionally allow for nonexperts to carry out very sophisticated computer simulations. Whereas there is a long tradition in the organometallic community of embracing theoretical concepts such as ligand field theory, MO theory or Marcus theory, the modern methods of computational molecular modeling have created a set of unique challenges. The numerical results of these simulations often require a careful inspection to ensure that they are interpreted correctly. As with any scientific equipment, quantum chemical modeling software assumes that the operator is aware of intrinsic limitations of the methods employed. In this tutorial, we review problems that often arise when using computer models to study organometallic reaction mechanisms.

In general, there are two categories of errors that are most often encountered. (*i*) *Errors arising from misunderstandings of the model chemistry.* These problems are not technical in the sense that they are independent of the choice of technical details and other technical settings of the calculation. Rather, these errors are systematic, because they reflect on the chemical process underneath the computer model. As such, these errors can be avoided by understanding how energies are computed and consistently applying a set of rules and practices. The aim of this tutorial is to provide an intuitively comprehensible explanation for some of these common problems and to discuss practical solutions for them. (*ii*) *Errors originating from technical aspects of the quantum chemical model.* The overwhelming majority of studies use density functional theory (DFT). The choice of the exchange-correlation functional can cause significant variations in the results, some of which can be anticipated easily, such as when spin-state changes or when van der Waals (vdW) interactions become important. Errors associated with these choices may be collectively regarded as technical errors. Minimizing these errors for various applications is an intensively pursued goal in computational method development, and there are many publications that can aid practicing computational inorganic chemists to choose appropriate computational methods for the specific problem of interest.[1]

Whereas much could be said about the choice of the computational parameters, the most practical, albeit opportunistic, approach for practicing organometallic chemists is to choose one of the many leading computational organometallic research groups and simply employ the identical technical parameters that they utilized in studies that are most relevant to the specific problem at hand. In this tutorial, we will concentrate on problems arising from misunderstandings of the model chemistry, because they have rarely been explained specifically and clearly in the literature and have led to numerous misinterpretations that can be found in the published literature.

■ THE TUTORIAL

Energies. A de facto standard adopted over the past decade in the organic and organometallic research communities is to use the solution-phase Gibbs free energy $G(\mathrm{sol})$ to construct energy profiles and investigate reaction mechanisms.[2] Once the structures of intermediates and transition states are optimized, the electronic energies can be evaluated. In DFT calculations, the combination of the exchange-correlation functional and the basis set is important in determining the quality of the results. B3LYP[3] has been and remains the most widely used functional,

Received: July 3, 2018
Published: September 24, 2018

DOI: 10.1021/acs.organomet.8b00456
Organometallics 2018, 37, 3228–3239

but newer functionals such as the Minnesota functional M06[4] have become very popular.

The computational efficiency, i.e. the time needed to complete a calculation, is very much dependent on the basis set size. Whereas larger basis sets will deliver more reliable results, the typical size of molecules of interest in organometallic research demands a compromise between technical sophistication and computational cost. One such compromise is to use a double-ζ basis set such as 6-31G** in combination with a compatible basis set, e.g. LACVP,[5] that include pseudopotentials for the transition metals. Optimizing geometries routinely at a higher level basis than double-ζ is not practical. Although this protocol has been shown to deliver reasonable geometries, it is often found that the energies computed using double-ζ basis sets are not always reliable. A reasonable workflow is to reevaluate the electronic energy of the computed intermediates and transition states with a larger basis set, such as cc-pVTZ(-f)[6] and keep the rest of the free energy components computed with the double-ζ basis set.

To derive entropy corrections, translational, rotational, and vibrational partition functions must be evaluated. Whereas the first two can be calculated by assuming simple models of a free particle in space and a rigid rotor, the vibrational entropies require the vibrational frequencies, which must be calculated explicitly. These are computationally expensive calculations but are now considered necessary. They also allow for obtaining vibrational zero-point energies, which can be used to more accurately estimate the enthalpy, and offer the additional benefit of judging whether a true local minimum and a saddle point on the potential energy surface have been obtained for intermediates and transition states, respectively. Reactants and intermediates must only display real frequencies, which are typically denoted as positive frequencies, whereas a transition structure must show one imaginary frequency that is associated with the atomistic motion along the bond that is formed or broken.

The solvation free energy $G(\text{solv})$ is routinely computed to account for solvation effects and is added to the gas-phase free energy, which results in the solution-phase free energy $G(\text{sol})$ of the molecule. The vast majority of studies utilize implicit models where the solvent is represented as a continuum dielectric field.[7] Unfortunately, the capability of these solvation models has often been subject to misinterpretations and misunderstandings. Thus, these problems are discussed in detail below. On incorporation of all of these components, the Gibbs free energy of a designated reactant, intermediate, and transition structures in the gas phase is given by

$$H(\text{gas}) = E(\text{SCF}) + \text{ZPE} + \int C(T)\ \mathrm{d}T \tag{1}$$

$$G(\text{gas}) = H(\text{gas}) - TS(\text{gas}) \tag{2}$$

where $H(\text{gas})$ is the gas-phase enthalpy of the molecule, $E(\text{SCF})$ is the calculated electronic energy by the self-consistent field (SCF) method, ZPE stands for zero-point energy, $C(T)$ is the heat capacity, T is the absolute temperature, $G(\text{gas})$ is the Gibbs free energy in the gas phase, and $S(\text{gas})$ is the total entropy of the molecule. The contribution from the integral of heat capacity is relatively small in comparison to other contributions and tends to be nearly constant for molecules of similar composition. As a result, these values often cancel when relative energies of the same molecule during a reaction are calculated. For this reason, this component is often omitted. $S(\text{gas})$ consists of three components, as mentioned above:

$$S(\text{gas}) = S_{\text{trans}} + S_{\text{rot}} + S_{\text{vib}} \tag{3}$$

where S_{trans}, S_{rot}, and S_{vib} are the translational, rotational, and vibrational entropies in the gas phase, respectively. Finally, the addition of the solvation free energy $G(\text{solv})$ affords the solution-phase Gibbs free energy:

$$\begin{aligned} G(\text{sol}) &= G(\text{gas}) + G(\text{solv}) \\ &= E(\text{SCF}) + \text{ZPE} - TS(\text{gas}) + G(\text{solv}) \end{aligned} \tag{4}$$

One question raised regularly is whether it is appropriate to add translational and rotational entropies computed under vacuum, since molecules are not free to move or rotate in the solution phase. It is correct that the translational and rotational degrees of freedom of a molecule are severely reduced in the solution phase, and it would be wrong to assume that the gas-phase entropies can be used to capture the solution-phase entropy. As outlined in eq 4, the solution-phase free energy $(G(\text{sol}))$ is estimated as the sum of the gas-phase free energy and the free energy of solvation. Thus, loss of translational and rotational entropy due to solvation is included in the free energy of solvation $G(\text{solv})$ and not adding gas-phase entropy corrections $(S(\text{gas}))$ when calculating the gas-phase free energy will lead to inconsistencies and noncancelling errors. Continuum solvation models are trained against experimentally determined free energies of solvation, and it is fundamentally impossible to divide the calculated solvation energy into their enthalpic and entropic components.

Translational Entropy. The concept of entropy is explained in introductory chemistry classes often using the example A → B + C vs A + B → C, where it is made clear that the first reaction is entropically favored over the second. More specifically, this example is the demonstration of the translational entropy. The simplest way of calculating the translational entropy is using the Sackur–Tetrode equation.[8] Whereas this equation is strictly only valid for monatomic species and assumes ideal gas conditions, the general trends and lessons that can be derived from this simple model are fully valid for more complex molecular systems. Of note, modern computational chemistry software packages compute the Sackur–Tetrode equation automatically when they carry out thermochemistry analysis. In its simplified form, the translational entropy can be written as

$$S_{\text{trans}} = \frac{3}{2}R\ \ln M + \frac{5}{2}R\ \ln T - 2.315 \tag{5}$$

where R is the ideal gas constant. The only variables are the mass and the temperature. It is instructive to inspect specifically how the translational entropy contributions to the free energy changes with the mass of the particle. Figure 1 shows the computed values for three different temperatures: 25 °C (298.15 K), 100 °C (373.15 K), and 300 °C (573.15 K). For a hydrogen atom, the $-S_{\text{trans}}$(298.15 K) value is −7.7 kcal/mol and the logarithmic dependence on mass gives the asymptotic progression that can reasonably be estimated to be approximately −11 kcal/mol for heavier particles. The dependence on temperature is also logarithmic, and it is fair to approximate that the translational entropy corrections are roughly −15 kcal/mol at 100 °C and −25 kcal/mol at 300 °C for nearly all particles. Thus, to a first-order approximation, it can be stated that a reaction A → B + C is entropically favored by −11, − 15, and −25 kcal/mol at 25, 100, and 300 °C, respectively, while the reaction A + B → C is disfavored by the same amount.

DOI: 10.1021/acs.organomet.8b00456
Organometallics 2018, 37, 3228−3239

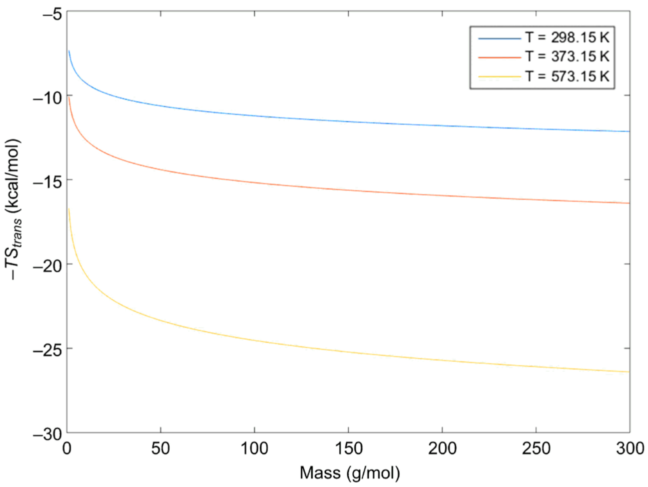

Figure 1. Translational entropy of a molecule at varying temperatures.

To illustrate this point, we calculated the free energies of formation of three molecules explicitly: (a) borazane, (b) ferrocene, and (c) tris(2,2′-bipyridine)cobalt(II) ($[Co(bpy)_3]^{2+}$), as shown in Figure 2; the energies are summarized in Table 1. For borazane, 1 equiv of borane is brought together with 1 equiv of ammonia. The total gas-phase entropy change associated with this reaction is 11.1 kcal/mol, whereas the net change of translational entropy is 9.6 kcal/mol. The formation of ferrocene from two cyclopentadienyl anions and an Fe(II), representing an association of three molecular fragments to a single molecule, affords an entropic penalty of 24.3 kcal/mol and a translational entropic penalty of 21.9 kcal/mol. Finally, the formation of $Co^{II}(bpy)_3^{2+}$ from three bipyridine ligands and a Co(II) ion requires an entropic penalty of 31.6 kcal/mol, where 34.8 kcal/mol is due to a translational entropy penalty. From these observations, we may conclude that the translational entropy is the dominant contributor to these reactions and they can be easily estimated and understood. A reaction that combines two molecular fragments into one experiences an entropic penalty of ∼11 kcal/mol, whereas reactions that combine three and four fragments into one molecule will be entropically disfavored by ∼22 and ∼33 kcal/mol, respectively.

Whereas the translational entropy corrections discussed above are easy to understand, they can lead to some nontrivial errors. Figure 3 compares the computed Gibbs free energy profile of a simple Diels−Alder reaction between 1,3-butadiene (**1**) and ethylene (**2**). Typically, the energy at the reactant state is taken as the sum of free energies computed separately for the reactants **1** and **2**, shown at 0.0 kcal/mol in Figure 3. The solid curve in Figure 3 represents the computed Gibbs free energy of the cycloaddition reaction. The translational entropies of the diene and the dienophile are 11.3 and 10.7 kcal/mol, respectively. The Gibbs free energy of the transition state **3-TS** is 36.8 kcal/mol, indicating that this reaction is exceedingly slow. The formation of the product, cyclohexene (**4**), is exothermic by 12.9 kcal/mol. Here, we utilize water (ε = 78.4) as the solvent represented by its dielectric constant. While this solvent is of course not realistic for the reaction, since neither 1,3-butadiene nor ethylene is sufficiently soluble in water, we use the water solvent for demonstrative purposes (vide infra). The computed Gibbs free energies of the transition state and the product are reasonable and are well within the expected range of what has been reported previously.[9] A trivial, yet serious, mistake can be made by combining the two reactants to a weakly interacting reactant complex and calculating its free energy as a single particle. The quantum chemical modeling software will treat this reactant complex as a single particle regardless of how weak the

Table 1. Molecular weight, $-TS$(gas), and $-TS_{trans}$ Values of the Structures (a) BH_3NH_3, (b) Ferrocene, and (c) $[Co(bpy)_3]^{2+}$, Respectively[a]

	(a) BH_3NH_3			
	(i) BH_3	(ii) NH_3	(iii) NH_3BH_3	(iii) − [(i) + (ii)]
MW	13.83	17.03	30.87	0.00
$-TS$(gas)	−14.48	−14.36	−17.75	11.09
$-TS_{trans}$	−10.10	−10.27	−10.82	9.55
	(b) Ferrocene			
	(i) Fe(II)	(ii) Cp^-	(iii) Fc	(iii) − [(i) + 2(ii)]
MW	55.85	65.10	186.04	0.00
$-TS$(gas)	−11.32	−18.74	−24.77	24.03
$-TS_{trans}$	−11.32	−11.46	−12.39	21.85
	(c) $[Co(bpy)_3]^{2+}$			
	(i) Co(II)	(ii) bpy	(iii) $[Co(bpy)_3]^{2+}$	(iii) − [(i) + 3(ii)]
MW	58.93	156.18	527.48	0.00
$-TS$(gas)	−11.37	−26.31	−58.73	31.57
$-TS_{trans}$	−11.37	−12.24	−13.32	34.77

[a]Entropies are computed at 298.15 K. Energies are given in units of kcal/mol. Abbreviations: Cp^- = cyclopentadienyl ligand, Fc = ferrocene, bpy = bipyridine, MW = molecular weight.

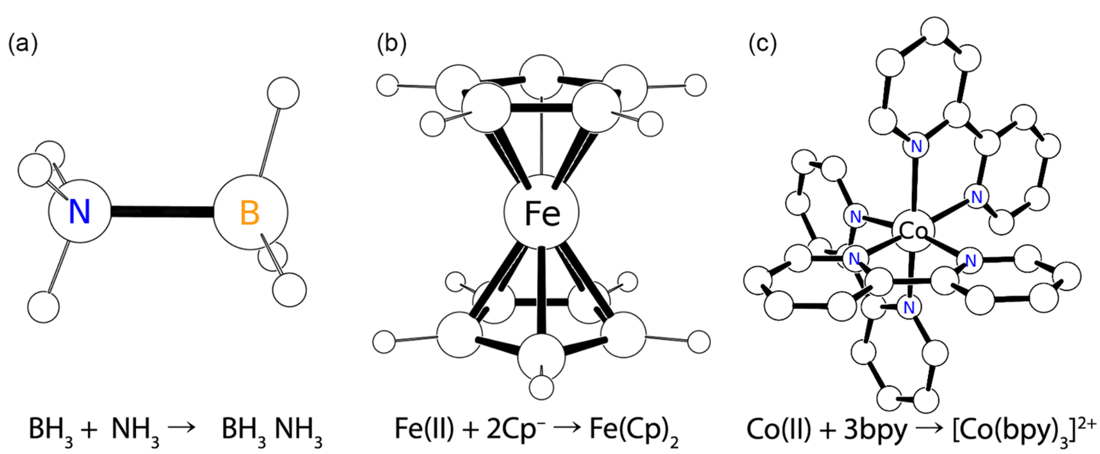

Figure 2. Structures of (a) BH_3NH_3, (b) ferrocene, and (c) $[Co(bpy)_3]^{2+}$. For (c), hydrogen atoms are omitted for clarity.

DOI: 10.1021/acs.organomet.8b00456
Organometallics 2018, 37, 3228−3239

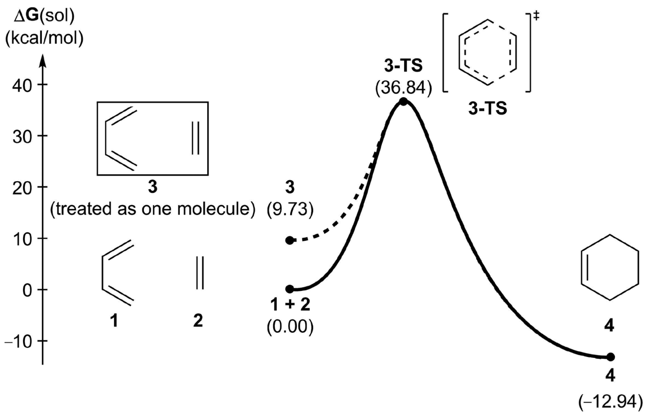

Figure 3. Diels−Alder reaction of 1,3-butadiene and ethylene: correct (solid curve) and an incorrect (dashed curve) computations. The solvation effect of solvent medium (water, $\varepsilon = 78.4$) was incorporated using an implicit solvation model (PCM).

interaction between them is, and the translational entropy penalty for having brought together two independent particles to form this weakly interacting complex will not be applied properly. When the transition state energy is compared to this new reference state, one may obtain a much lower barrier of 27.1 kcal/mol. The difference in the computed Gibbs free energies of the transition state and the product amount to ∼10 kcal/mol, which is of course easy to understand with the aforementioned trends.

Adding Explicit Solvents. Computationally modeling solvation effects is challenging, because several nontrivial interactions between the solvents and the solute molecules, including hydrogen bonds, van der Waals, and electrostatic interactions, and the ensemble-average over a very large number of possible structures determine the final solvation energy. Since the individual solvent−solute interactions are weak, often being not greater than a few kcal/mol, they cannot be considered stable at room temperature and they will constantly break and re-form. Thus, the simplistic, but on first sight plausible, idea that one may simply add a few solvent molecules to the molecule of interest and optimize the geometry of such a solvent−solute complex and then estimate the solvation energy as a "solvent binding energy" is fundamentally flawed. If such an explicit solvation model is to be constructed, it is necessary to carry out a molecular dynamics simulation with a sufficiently large number of solvent molecules, sample a statistically representative number of structures, and ensemble-average over these structures, as is done in protein modeling studies employing computationally more tractable molecular mechanics methods. For typical organic and organometallic systems, such properly constructed explicit solvation models are technically out of reach due to unreasonable computational cost. Given these intrinsic challenges, the performance of implicit solvation models that originate from the Born-Onsager concept of solvation, where the solvent medium is treated as a continuum dielectric field, is remarkable. Nowadays, the polarizable continuum model (PCM) and the variants of the model are readily available in quantum chemistry packages and are utilized by many practitioners. With the choice of dielectric constant that matches with the solvent medium used, one can compute G(solv) with ease. For interested readers, we refer to several methodological studies that discuss the details of the available continuum treatment of solvation effects.[7,10]

These fundamental concerns notwithstanding, adding a few solvent molecules to the solute and applying a continuum solvation model to such a solvent−solute cluster, continue to be appealing and studies can be found reporting such hybrid models for reaction mechanisms. The energies obtained by these hybrid models must be evaluated carefully. To demonstrate how systemically unreliable these hybrid models can be and to highlight the fundamental reasons for why these energies cannot be trusted, we constructed a simple illustrative example.

Figure 4 shows the reaction energy profile of the simple Diels−Alder reaction discussed above using 1,3-butadiene and ethylene as a black line. To this simple reaction model, we added three water molecules. Avoiding the translational entropy error

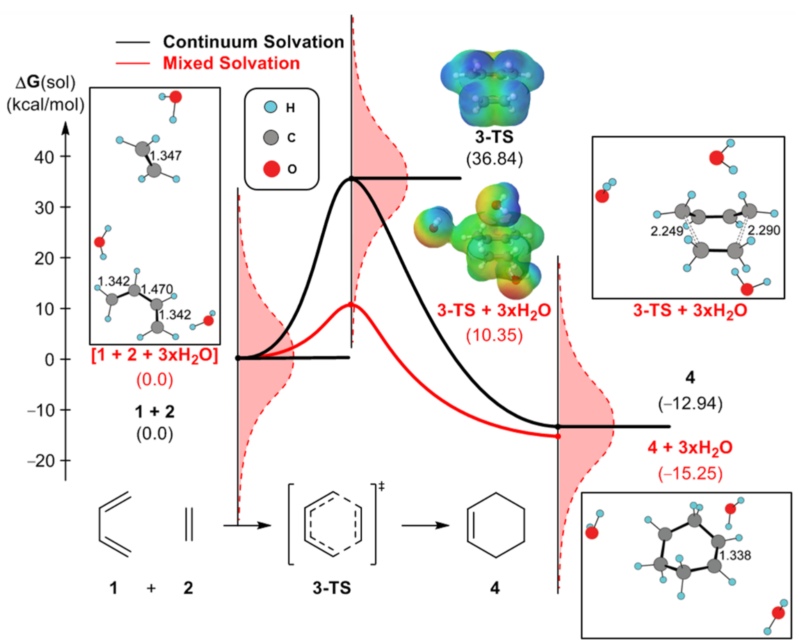

Figure 4. Diels−Alder reaction of 1,3-butadiene and ethylene under continuum and mixed solvation conditions. All bond lengths are given in Å. The solvation effect of solvent medium (water, $\varepsilon = 78.4$) was incorporated using an implicit solvation model (PCM).

DOI: 10.1021/acs.organomet.8b00456
Organometallics 2018, 37, 3228−3239

we discussed above, we may get the proper free energy for this cluster model, shown as a red line. As discussed above, the three explicit solvents can adopt many different structures, which will have different energies, and to properly account for the flexibility of the solute−solvent interaction, a statistically representative number of these structures must be sampled. Assuming that the continuum solvation model captures the energies of the reactants correctly, the solute−solvent cluster model may produce an energy distribution shown by the light red distribution curve, centered around the continuum solvation energy value. By simple placement of the three water molecules at random or by some intuitive expectation, it is not possible to capture the ensemble-average structure. Note that the error described here is due to the fact that a static DFT-optimized geometry is not capable of capturing the ensemble-average structure. This is a systemic, conceptual error that cannot be remedied by a more careful evaluation of the cluster formation energy. We mention that the cluster formation energy based on static, 0 K optimizations can be made more accurate by correcting for several technical errors. For example, one can estimate the error that arises from the basis set being too small and atom-centered via a standard technique called basis set superposition error (BSSE).[11] In addition, one could also correct for concentration effects, as detailed elsewhere in this tutorial. However, none of these technical improvements remedy the fundamental issue that a static geometry optimization involving very weak interactions does not afford a reliable average structure that is needed.

To illustrate the issue and initiate an internal reference, we placed the [**1** + **2** + $3H_2O$] state at 0 kcal/mol to become the reference state for this hybrid model, illustrated in Figure 4. In reality, it is unlikely that the structure produced with three water molecules placed at random represents an ensemble-averaged structure. As the calculated structure in Figure 4 shows, the three water molecules are at random positions.

When carrying out the transition state search, one would again have to ensemble-average over many configurations to obtain a different average solvent structure that is appropriate for the transition state. By a simple carrying of the initial reactant structures of the explicit solvents over to the transition state as initial guesses, it is unlikely that the appropriate new solute arrangement will be found. Instead, it is much more likely that a solvent arrangement that is much higher or much lower in energy than the average structure will be located in the standard geometry optimization. In our example, we found a structure that gave a much lower energy, as illustrated in Figure 4. By simply adding the three water molecules, we were able to find a solvent−solute cluster at reactant and transition states that are 10.3 kcal/mol away from each other, whereas the continuum solvation model shows 36.8 kcal/mol. The 26.5 kcal/mol of energy difference stems from both translational entropy (∼10 kcal/mol) as mentioned above and the three arbitrarily placed water molecules. As can be seen from the illustration of the transition state structure with the three water molecules, they are not bound in a special way, nor do they provide some nontrivial assistance. Instead, they are just as randomly oriented as they were in the reactant. The point here is that, because these structures are not uniquely determined, they will create noncanceling errors in energy between them.

As illustrated in Figure 4, the relative energy can be changed dramatically by placing the water molecules at different positions. That is, by not averaging over all the possible arrangements but picking a specific structure, we can access any of the energies within the range of the light red distribution curves. Obviously, a reaction barrier of 10.3 kcal/mol would indicate that the Diels−Alder reaction of butadiene and ethylene should be exceedingly fast at room temperature in water. This is obviously a nonsensical conclusion and is an artifact of the model we show above. Unfortunately, explicit solvents are typically added to a computer model when the simple continuum model treatment does not afford the barriers expected. In such a case, researchers tend to add solvent molecules with some justification and repeat the energy profile search. Typically, the search is continued until the expected result is recovered, and to make matters worse, additional solvent molecules are sometimes added if no satisfactory energy is found. Admittedly, the water molecules in our example were placed without any chemically intuitive justification, which led to an exaggerated noncanceling error for illustrative purposes. Whereas a more purposeful placement of explicit solvent molecules can be imagined that will seemingly reduce the error, in reality, the noncanceling errors between these nonrepresentative reactant conformers and those found for transition states persist and the energy differences cannot be trusted. The only remedy is to find a representative average structure where error cancellation is possible. Energies obtained from these hybrid models must be evaluated with caution, in any case.

Of course, there are reactions where specific solvent molecules do not behave like the bulk solvent and participate in a chemical reaction actively, for example by becoming a ligand, and in those cases, the reaction mechanism cannot be properly modeled without considering a solvent molecule specifically. In these cases, the solvent−solute interactions are much stronger: e.g., because one solvent molecule becomes a ligand. However, in general, mixing implicit solvation models with solvent−solute cluster models of solvation is a problematic proposition and must be done carefully. This was demonstrated by Houk and co-workers, who sampled 100 configurations of the transition structures with the surrounding solvent in order to reduce the statistical errors to less than 2.0 kcal/mol in a study of the mechanistic details of SpnF enzyme catalyzed cycloaddition.[12]

Global vs Local Minima. The problem of capturing chemically appropriate and representative solvent−solute structures mentioned above is a special case of a longstanding general problem in computational chemistry. Because standard geometry optimization strategies start from a given initial guess geometry and search for a lower energy structure by relatively small modifications, the optimized structures of all intermediates and transition states are necessarily local solutions, and it is impossible to know if the most appropriate structures for intermediate and transition states have been captured. Locating global minima in computer simulations is an active area of research and represents a serious problem that is far from being solved.[13] For most organometallic reactions, two strategies proved useful. First, much structural information is available for most fragments encountered in organometallic complexes that can be accessed conveniently through the Cambridge Crystal Structure Database.[14] With use of typical bond lengths and bond angles for molecular fragments from the database, high-quality geometries can be generated even for unprecedented complexes that will afford reasonable structures. Another helpful strategy is to employ classical methods of structure and bonding that have a long tradition in organometallic chemistry, such as ligand field theory, valence shell electron pair repulsion, and formal valence electron counting rules. When these methods are combined with the extensive empirical knowledge of which structural motifs are

DOI: 10.1021/acs.organomet.8b00456
Organometallics 2018, 37, 3228−3239

commonly seen for which metal in a given oxidation state that the organometallic research community has assembled over the last century, it is possible to propose very reasonable structures for most intermediates and transition states encountered in organometallic reactions. These traditional, albeit empirical, rules are powerful when they are combined with precise quantum chemical calculations, as unusual and surprising features of a reaction can be identified and analyzed, in addition to providing reasonable guesses for quantum chemical refinement.

In principle, the empirical bias mentioned above can be avoided by carrying out Monte Carlo or molecular dynamics simulations to broaden the configurational space and increase the number of structures that are explicitly considered. Whereas such an approach that is computationally much more demanding seems more rigorous and preferable, it is not clear that these methods will necessarily afford higher quality results for practical purposes. Because of the flexible electronic nature of the transition-metal centers, the number of structural isomers that are energetically close to each other is much greater than that for typical organic systems. In particular, first-row-metal systems can adopt various spin states within a narrow energy range that makes it very challenging to properly model these states and assign their energies correctly within the necessary level of accuracy. Undoubtedly, the success of DFT models of organometallic reactions relies heavily on error cancellation and capture of the key elements of the chemical reactions in an approximate, but appropriate, way. Thus, incorporating empirical knowledge and structural features from prior experience is a much more important strategy than is commonly acknowledged.

Solution-Phase Structures and Spectra. All standard quantum chemical methods optimize the geometry of molecules under vacuum, i.e. no environmental effects are included, but the majority of experimental information on molecular structures originates from single-crystal X-ray diffraction studies. It is generally found that DFT-generated bond lengths and angles are in good agreement with the experimental data from the solid state. This agreement has traditionally served as a key benchmark for calculations. Since nearly all modern quantum chemical packages offer continuum solvation models, a question that arises often is whether these solvation models can be employed to obtain solution-phase structures. The motivation is of course to prepare a more realistic computer model. Similarly, it is tempting to calculate vibrational frequencies, UV/Vis absorptions, and other molecular properties in the solution phase. The key question is whether continuum solvation models are capable of capturing how solvation affects these experimental observables.

For geometry optimizations, there are cases where the continuum solvation model affords chemically meaningful results. One such example is fluorescein, which exists in various states of protonation depending on the pH and adopts different tautomeric forms, which can affect the strong and characteristic green fluorescence. Most notably, the highly fluorescent neutral form exists as a zwitterion in solution, where the carboxylate of the benzoate fragment carries a negative charge and the xanthene moiety is positively charged. As illustrated in Figure 5, the zwitterionic form is not a local minimum under vacuum and a standard geometry optimization yields the closed lactam form with a C−O distance of 1.496 Å. The continuum solvation model can stabilize the zwitterion, and the geometry optimization with the continuum solvation potential switched on gives a structure where the C−O distance is 2.379 Å. Experimentally, the lactam structure is observed in the solid state. Although it appears in this case that the continuum solvation model can

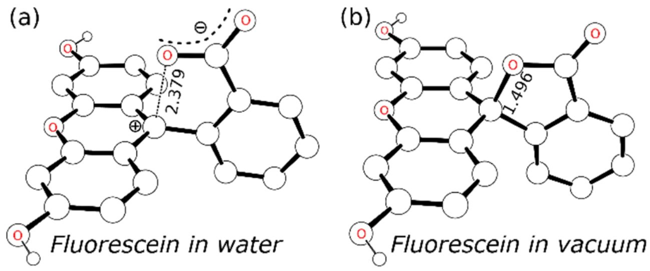

Figure 5. Optimized geometries of fluorescein (a) in an implicit solvent environment and (b) under vacuum. The B3LYP-D3/DZP levels of the theories were employed to compute the geometries, with the COSMO implicit solvation model used to represent the aqueous environment in (a). Nonessential hydrogen atoms are omitted for clarity. Bond lengths are given in Å.

capture the structural changes upon solvation, it is important to realize that this is an exceptional and trivial case where the continuum solvation model captures the main feature of structural change.

Fundamentally, there are several reasons to be critical about carrying out geometry optimization with the continuum solvation model. First, to obtain physically meaningful structural changes upon solvation, the modifications to the model potential must contain some concept that will lead to a physically meaningful distortion in the structure. Continuum solvation models work with a fictitious surface representation of the solute that is used to produce a dielectric response field as a function of the partial charge distribution of the solute molecule. The solvation energy is highly dependent on the size and shape of the surface representing the solute. To obtain reasonable solvation energies, the atomic radii employed to construct these surfaces have been carefully adjusted and parametrized to match the experimental solvation energies. This procedure is highly empirical, and the parameters have no physical meaning. They are oversimplified fit parameters that reduce the complexity of individual solvent−solute interactions such as hydrogen-bond, dipole−dipole, and van der Waals interactions into a fictitious surface potential, the physical meaning of which derives from being scaled to reproduce the experimental solvation free energies. During this model construction and parameter fitting process, no information about the structural change is included. It is extremely challenging to obtain highly precise and reliable structural data in the solution phase experimentally. Thus, even if the continuum solvation model could be reformulated to incorporate information about the shape change of the molecular potential energy, the experimental data needed to train such a model would be insufficient and inadequate.

Similar arguments can be constructed for employing continuum solvation models for calculating various spectroscopic features. For electronic transitions, the frontier orbital energy changes as a result of solvation must be properly captured. Understanding solvatochromism is challenging and requires understanding how the dipole moments of the ground and excited states are affected by the solute−solvent interactions, which are intrinsically dynamic processes, as mentioned above. The idea that a simplistic Onsager model trained to reproduce the solvation energy of a handful of test molecules is capable of capturing these complex processes to any chemically meaningful extent is not reasonable. Although there will be cases where seemingly plausible results can be obtained by "simply trying", employing continuum solvation models for anything more than solvation energy calculations requires some

DOI: 10.1021/acs.organomet.8b00456
Organometallics 2018, 37, 3228−3239

caution and the realization that there is no justification for doing so.

Vibrational Entropy Corrections. Vibrational modes and frequencies are computed routinely using the harmonic oscillator model, which allows for derivation of the vibrational entropy corrections. The vibrational entropy of a molecule is given by

$$TS_{\mathrm{vib}} = -RT\ \ln(1 - \mathrm{e}^{-hc\tilde{\nu}/RT}) + hc\frac{\tilde{\nu}\mathrm{e}^{-hc\tilde{\nu}/RT}}{1 - \mathrm{e}^{-hc\tilde{\nu}/RT}} \tag{7}$$

where S_{vib} is the vibrational entropies of the molecule, R is the ideal gas constant, T is the absolute temperature, h is the Planck constant, and $\tilde{\nu}$ is the wavenumber of the vibrational mode.

Figure 6 shows the contribution of vibrational modes of different energies at a given temperature. It is easy to see that

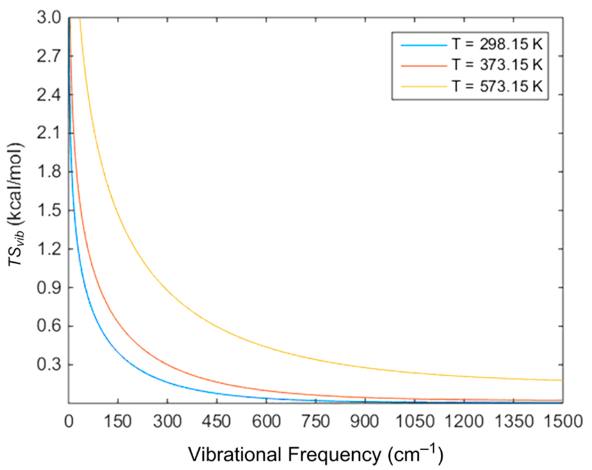

Figure 6. Plot of TS_{vib} versus wavenumber.

vibrational modes below 150 cm^{-1} contribute a significant amount to the Gibbs free energy changes, whereas higher energy vibrations have small to no contribution to the vibrational entropy. Close to 0 cm^{-1} very small changes in frequency translate to relatively large changes in entropy corrections. This trend is worrisome because many low-energy modes often arise from computational artifacts and are chemically not meaningful. Those low-energy modes include transverse vibration of linear molecules and rotation of a large substituent across a sp^3–sp^3 bond; neither of them are relevant to the stability of molecules that are subject to a computational analysis. For that reason, one option utilized in quantum chemical programs is to discard these extremely low frequencies when the vibrational entropy is computed. Another perhaps more robust practice is replacing all frequencies below 50 cm^{-1} by 50 cm^{-1}—Cramer[15] had suggested to replace all frequencies below 100 cm^{-1} by 100 cm^{-1}, which in our own experience is slightly too stringent and can give rise to unintended artifacts. As explained above, these low frequencies result in entropy contributions of 1−2 kcal/mol at room temperature. While these absolute values may seem small, they can cause inconsistencies, because many quantum chemical packages define a threshold value for physically meaningful vibrational frequencies that are employed for computing thermodynamic parameters. These default thresholds range from 10 to 50 cm^{-1} in commercial programs, and in cases where these low-energy frequencies slip below the threshold during a chemical reaction, physically meaningless energy jumps can be the result due to simple neglect of these low-frequency vibrations. Vibrational frequency changes of a few wavenumbers are not meaningful, as they are associated with less than 0.1 kcal/mol—it is for that reason that simply equating all frequencies lower than 50 cm^{-1} to 50 cm^{-1} may produce a consistent set of energies that allows for a systematic error cancellation. In conclusion, it is important to inspect the computed vibrational frequencies in calculations and be alerted when particularly low frequencies are computed, as we highlight below.

Figure 7 illustrates the entropy contributions of a low-frequency vibration in a $\mathrm{CpRh^{III}}$ complex associated with the rotation of the cyclopentadienyl ligand. By rotating the cyclopentadienyl ligand, one can tune the lowest vibrational wavenumber from 9.5 to 23.0 cm^{-1}. Table 2 shows computed free energy components of the model system. As we rotate the cyclopentadienyl ligand in a clockwise or anticlockwise direction, the vibrational contribution to the Gibbs free energy rises from −54.9 to −53.1 kcal/mol (Figure 7b), resulting in 2.0 kcal/mol in total variation of the Gibbs free energy. On moving from **A** to **G** via **D**, the electronic energy varies only by 0.4 kcal/mol.

These physically meaningless energy changes can be misleading. Figure 8 illustrates the free energy profile of a Rh(III)-catalyzed 7-azaindole synthesis that utilizes 6-methoxyamidopyridine as the substrate.[16] In the reaction, the alkyne undergoes migratory insertion to give an eight-membered rhodacycle intermediate. The orientation of the inserted alkyne determines the regioselectivity, and this is a classical example of a reaction where **5-TS-6**, shown in red, is sterically less demanding than **5-TS-7**, shown in blue, as illustrated in Figure 8b. Visual inspection of the transition-state structures clearly suggests a sterically more demanding geometry in **5-TS-7**, and the electronic energies, which should capture such a steric effect reliably, indicate that **5-TS-6** is 2.8 kcal/mol lower in energy. Consistent with this picture, 2-aryl-7-azaindole is obtained as the product in experiments, again suggesting that **5-TS-6** is the transition state leading to the product. In our initial computational analysis, we found that the vibrational entropy corrections invert the electronic ordering of the energies and predict that **5-TS-6** at 14.3 kcal/mol is 0.2 kcal/mol higher in energy than **5-TS-7′**, the transition state leading to the anticipated side pathway. For reactions that are basically identical, but only differ in the regiochemistry, such a reversal in energy ordering based on entropy corrections is unusual. Upon more detailed examination, we found that a very low frequency vibration at 8.24 cm^{-1} that is physically not meaningful was found for the transition state **5-TS-7′**, which contributed 3.0 kcal/mol to the Gibbs free energy of the transition state. This is of course a computational artifact that highlights the effect described above. By removal of the low-frequency vibrational mode when the entropy is computed, the activation energy of the transition state of the minor pathway (**5-TS-7**) shifts to 17.1 kcal/mol, which is consistent with the general expectation that vibrational entropy should not invert the energy ordering in reactions such as this and is confirmed by experiments.

Reaction Rates and Barriers. Computing the reaction energy profile and locating transition state structures that connect local energy minima have become standard in computational studies of organic and organometallic reactions. As the transition states cannot be detected experimentally, computational methods are helpful for obtaining precise structural and energetic information. To validate and benchmark these calculations, the measured rates are commonly compared to computed transition state energies. Initially, the relative Gibbs free energies (ΔG) of relevant intermediates and transition

DOI: 10.1021/acs.organomet.8b00456
Organometallics 2018, 37, 3228−3239

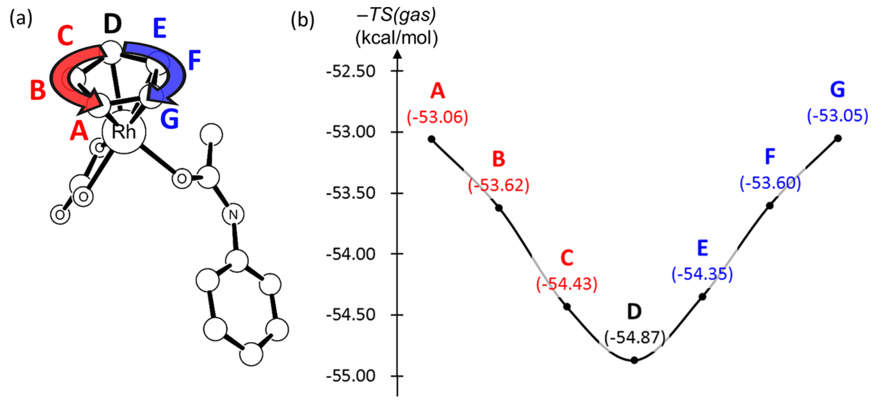

Figure 7. Structure of (a) $CpRh^{III}$ bound to an bicarbonate and an amidopyridine and (b) the computed vibrational entropic contribution ($-TS_{vib}$) depending on the rotation of Cp. Hydrogens are omitted for clarity. The solvation effect of the solvent medium (1,2-DCE, ε = 10.43) was incorporated using an implicit solvation model (PCM).

Table 2. Variation of Energy Component According to Rotation of Cp[a]

	A	B	C	D	E	F	G
ΔE(SCF)	0.39	0.12	0.00	0.00	0.00	0.09	0.35
ΔZPE	−0.11	−0.02	0.00	0.00	0.01	−0.02	−0.10
−TΔS(gas)	1.81	1.25	0.44	0.00	0.52	1.27	1.82
ΔG(solv)	−0.10	−0.13	−0.12	0.00	−0.09	−0.17	−0.19
ΔG(sol)	1.99	1.21	0.32	0.00	0.44	1.17	1.88
−TS(gas)	−53.06	−53.62	−54.43	−54.87	−54.35	−53.60	−53.05
Wave-numbers (cm^{-1})	22.97 37.26 42.65 72.48 73.44 94.06	19.94 36.51 41.12 45.04 73.16 90.68	16.47 19.21 36.02 41.03 73.06 88.81	9.52 17.96 36.26 41.06 73.15 88.56	17.39 20.19 36.18 41.22 72.99 88.72	19.96 36.47 41.53 46.18 73.15 90.48	22.86 36.97 43.49 73.24 73.57 93.72

[a]Energies are given in units of kcal/mol. The temperature is 363.15 K.

structures are computed. The Gibbs free energy of separated reactants or any intermediate whose presence is granted (i.e., precatalyst and substrate) can serve as the reference energy of the entire reaction energy profile. This is because the relative free energy, not the absolute energy, determines the relative concentration of intermediates and the rates of activation via transition states. The difference between the Gibbs free energy of the highest energy transition state and the lowest energy minimum preceding the transition state determines the overall activation barrier of a reaction, assuming that every step on the potential energy surface is reversible. The highest barrier is assumed to be associated with the slowest step in the reaction, which becomes the rate-determining step (RDS) in stoichiometric reactions or the turnover-limiting step (TLS) in catalytic reactions.

The activation energy of the rate-determining step/turnover-limiting step dictates the feasibility of the reaction mechanism at the temperature and pressure the experiments were conducted. The Eyring equation[17] correlates the activation energy ($\Delta G^{\ddagger}$) and the rate constant (k) of the RDS:

$$k = \frac{k_B T}{h} e^{-\Delta G^{\ddagger}/RT} \qquad (8)$$

Figure 9 illustrates the rate constants at different temperatures. At room temperature (298.15 K) and a barrier height of 25 kcal/mol, the rate constant is 0.011 mol h^{-1}, which is equivalent to 0.254 mol day^{-1}. As the barrier height increases to over 25 kcal/mol, the rate decreases exponentially to below 1 mol day^{-1}, suggesting that the reaction is too slow to be observed. It is instructive to bear in mind that at room temperature an activation energy barrier lower than 25 kcal/mol is viable and a higher barrier must be considered too high to give realistic rates. The elevation of the reaction temperature facilitates the reaction to occur, of course. At 373 K (100 °C), the rate constant associated with a 25 kcal/mol barrier height is 62.953 mol h^{-1}. Even at a 33 kcal/mol barrier, the rate is 0.001 mol h^{-1}, which can convert 1 mol of reactant after a few days. At 573 K (200 °C), even a 50 kcal/mol activation barrier can be overcome to produce a nearly completed reaction within 1 h.

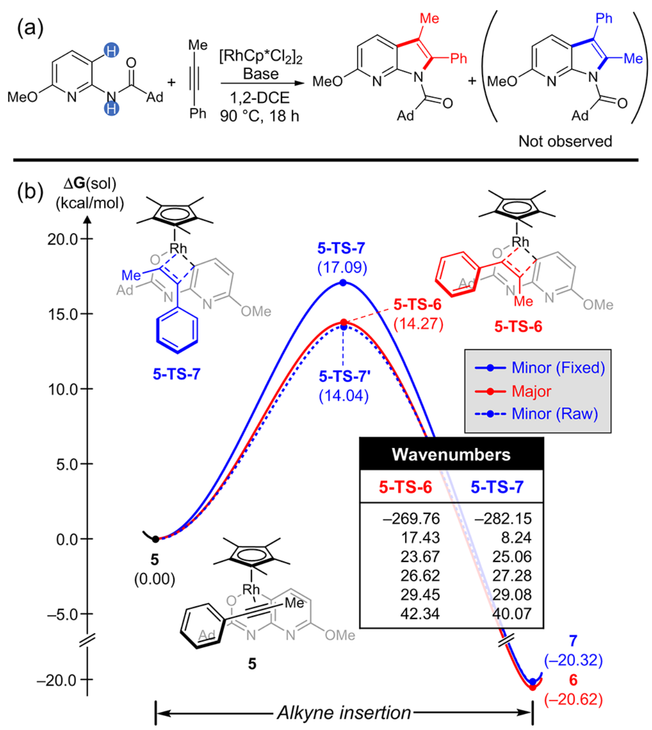

Figure 8. Reaction scheme of (a) Rh(III)-catalyzed 7-azaindole synthesis and (b) energy profile of the alkyne insertion step. The solvation effect of the solvent medium (1,2-DCE, ε = 10.43) was incorporated using an implicit solvation model (PCM).

Concentration Effects. Le Chatelier's principle is one of the most pervasive concepts in chemistry, which teaches about the

DOI: 10.1021/acs.organomet.8b00456
Organometallics 2018, 37, 3228−3239

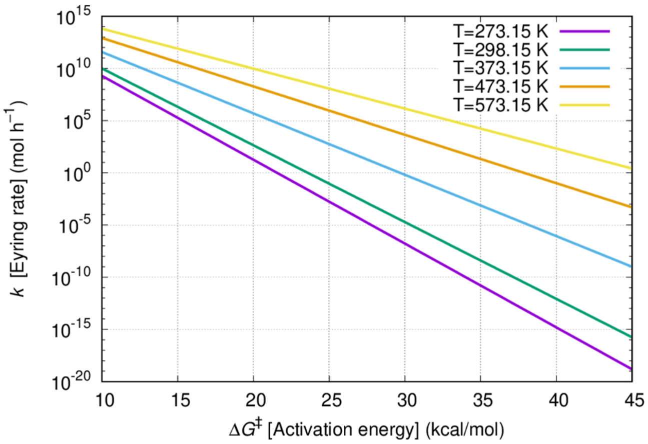

Figure 9. Plots of the rate constant (k) as a function of activation barrier $\Delta G^{\ddagger}$.

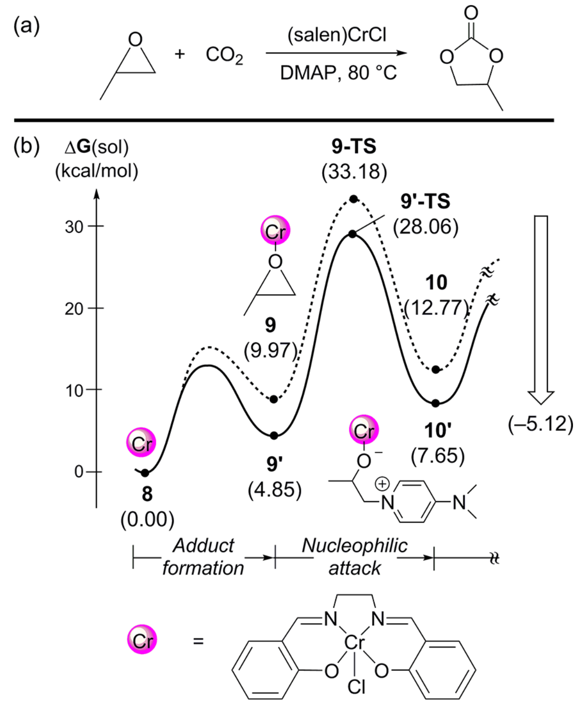

Figure 10. Reaction scheme of (a) Cr- and DMAP-cocatalyzed cyclic carbonate formation using epoxide and (b) CO_2 part of the energy profile of the reaction. A truncated catalyst is used for this calculation. The solvation effect of the solvent medium (dichloromethane, $\varepsilon = 9.08$) was incorporated using an implicit solvation model (PCM).

shift of equilibria in response to external changes including concentration, pressure, and temperature. Quantum chemical calculations are performed assuming a standard state that is ideally normalized. That is, when two reactants are brought together to react, the concentration is implied to be identical and normal: i.e., 1 M. The computed energies are most commonly not evaluated in a quantitative sense, and comparisons with experiments are difficult, since the concentrations of the active components in most experiments are not precisely known. Nonetheless, these standard-state effects can be significant in some cases, for instance when one of the reactants is used neat, so that its concentration is much higher than that of other components of the reaction. In these case, the computed energies can easily be adjusted to incorporate these effects. For an unimolecular reaction of a reactant in concentration [R] and a product in concentration [P], the Gibbs free energy of a reaction containing reaction quotient $Q = [P]/[R]$ is expressed as

$$\Delta_r G = \Delta_r G^\circ + RT \ln Q \tag{9}$$

where ΔG° is the computed Gibbs free energy when both the reactant and the product are equimolecular in concentration. Thus, the free energy correction due to a concentration differential can be added easily.

Figure 10 illustrates the reaction energy profile of a catalytic cyclic carbonate formation. Here, the epoxide reactant is given in 1500 times higher concentration in comparison to the catalyst.[18,19] In the Gibbs free energy profile, the dashed line represents the calculated free energy profile under equimolar conditions (CO_2:epoxide:catalyst = 1:1:1), whereas the solid line shows the energy profile that incorporates the experimental concentration ratio (1:1500:1)—in this case, we assume the effective concentration of CO_2 to be low. For our calculations we assume its concentration to be equal to that of the catalyst. The reaction quotient (Q) is used to quantify the Gibbs free energy change caused by the concentration gradient that is equivalent to 5.1 kcal/mol (eq 9). The Gibbs free energy of the highest barrier (**9-TS**) without consideration of the concentration gradient is 33.2 kcal/mol, which means that this barrier would be difficult to overcome under the given conditions. On the other hand, with proper consideration of the concentration ratio, the computed activation barrier (**9′-TS**) becomes 28.1 kcal/mol, which makes the proposed mechanism much more likely at slightly elevated temperatures.

Dissociation/Association Transition States. Establishing the transition state of a reaction where a simple bond is broken to give two dissociated fragments with minimal structural change is fundamentally difficult. To find transition states, the molecular potential energy surface (PES) is scanned for a saddle point. Specifically, the electronic energy surface is scanned. Very simple bond cleavage events are often not associated with such a saddle point on the electronic energy surface, which makes it impossible to locate these transition states. Consider the bond-dissociation trajectory of a hydrogen molecule starting from the equilibrium distance at which the electronic energy is lowest to the dissociation limit where the two hydrogen atoms are independent atoms. The electronic energy surface of this process is given by the familiar Morse function,[20] and there is no local maximum on the energy curve that connects the reactant and the product state. Instead, the energy increases monotonically to reach the bond dissociation limit. Of course, this fact does not indicate that the dissociation of the hydrogen molecule is barrierless. In comparison to the hydrogen molecule, the two hydrogen atoms in the product state have notably increased translational entropy. Thus, as the hydrogen molecule travels along the trajectory of bond breaking, the translational entropy increases and lowers the free energy by ~7–8 kcal/mol at room temperature in comparison to the enthalpy, as explained above. Thus, the transition state for such a process has a significant contribution from the change in entropy. Since conventional quantum chemical packages sample only the electronic energy surface, these transition states cannot be located. Fortunately, these transition states can be estimated easily and this fundamental problem is not a critical issue in most organometallic reactions. Often, simple product loss and substrate uptake reactions are subject to this issue and their transition states cannot be located, but they are noncritical in most cases.

In cases like this, a simple method can be used to estimate the bond dissociation barrier, as summarized in Figure 11.

DOI: 10.1021/acs.organomet.8b00456
Organometallics 2018, 37, 3228–3239

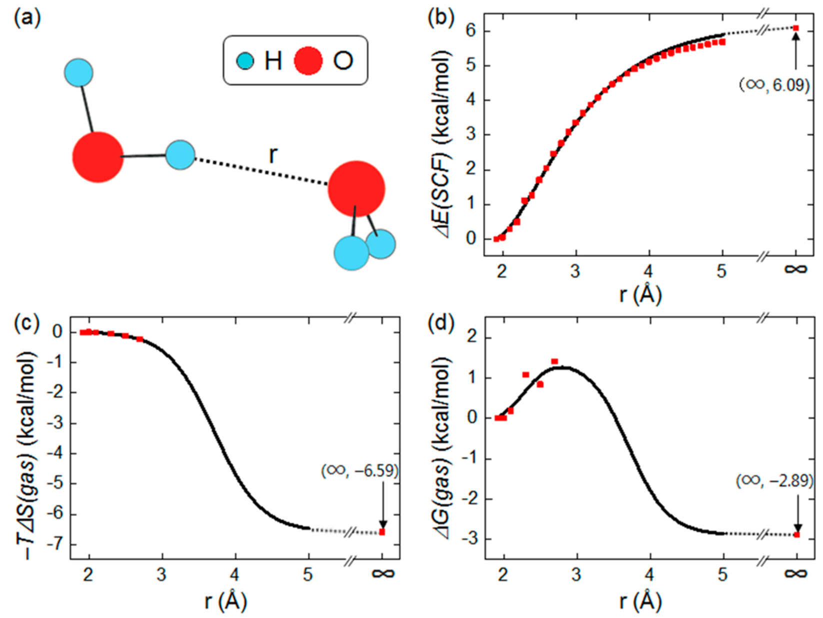

Figure 11. (a) Schematic illustration of a water dimer dissociation and the profiles of (b) computed electronic energies, (c) $-T\Delta S$, and (d) free energies in the gas phase.

We consider the hydrogen bond dissociation barrier of a water dimer in the gas phase. First, the electronic energy is determined by computing the energy of the water dimer at the fully optimized equilibrium geometry with an intermolecular hydrogen bonding distance of ~1.9 Å, followed by stepwise elongation of that hydrogen-bonding distance, as shown in Figure 11b. The value at infinite distance is taken as the energy of a single water molecule multiplied by 2. These electronic energies can be fit to a Morse function, as indicated in Figure 11b. Next, we calculate the entropy component $-T\Delta S$ at T = 298.15 K. Here, the entropy computed at the equilibrium geometry is meaningful and contains the translational entropy correction for a single molecular entity, the water dimer. As we elongate the bond and evaluate the entropy assuming the standard approximations explained above, the calculated entropy values become increasingly incorrect, because the treatment of a water dimer at a H···O distance of e.g. 3 Å as a single particle with the translational entropy of a single particle is not appropriate. However, the question of how to correct for this simple problem remains. One possible way is to compute the entropy for the first few elongation points, assuming that at infinite distance the entropy is simply the entropy of simple water molecules multiplied by 2 and then fit these data points to a sigmoidal function, as we highlight in Figure 11c. In this specific case, the entropy correction at infinite distance is −6.6 kcal/mol. The two fit functions can finally be combined to obtain the projected free energy profile, which of course will show an approximation for the saddle point. In the water dimer example, we find such a projected transition state at an energy of ~1.3 kcal/mol, as illustrated in Figure 11c. A similar method was previously used to estimate the depurination transition state of a platinated guanidine model to better understand the mechanism of action of cisplatin.[21]

■ COMPUTATIONAL METHODS

All geometry optimizations and frequency calculations except for fluorescein in Figure 5 were carried out using density functional theory[22] (DFT) as implemented in the Jaguar 9.1[23] suite of ab initio quantum chemistry programs. Geometry optimizations to the stationary points as well as the transition state (TS) optimization to the saddle points were performed[24] with the B3LYP[3] functional and the 6-31G** basis set.[25] Transition state structures were obtained from the quadratic synchronous transit (QST) search methods.[26] Cr, Fe, Co, and Rh were represented using the Los Alamos LACVP[5] basis that includes effective core potentials. The energies of the optimized structures were reevaluated by additional single-point calculations on each optimized geometry using Dunning's correlation consistent triple-ζ basis set cc-pVTZ(-f)[6] that includes a double set of polarization functions. For Cr, Fe, Co, and Rh, a modified version of LACVP was used in which the exponents were decontracted to match the effective core potential with triple-ζ quality. Analytical vibrational frequencies within the harmonic approximation were computed with the 6-31G**/LACVP basis to confirm proper convergence to well-defined minima on the potential energy surface. Solvation energies were evaluated by a self-consistent reaction field (SCRF) approach based on accurate numerical solutions of the Poisson−Boltzmann equation.[10] In the results reported, solvation calculations were carried out with the 6-31G**/LACVP basis at the optimized gas-phase geometry employing the dielectric constant of ε = 78.4 (water), 10.43 (1,2-DCE), and 9.08 (dichloromethane). As is the case for all continuum models, the solvation energies are subject to empirical parametrization of the atomic radii that are used to generate the solute surface. We employed the standard set of optimized radii in Jaguar for H (1.150 Å), B (2.042 Å), C (1.900 Å), N (1.600 Å), O (1.600 Å), Cr (1.511 Å), Fe (1.456 Å), Co (1.436 Å), and Rh (1.464 Å). Geometry optimizations of fluorescein were performed using the ADF 2017.105 modeling suite.[27,28] The geometry optimizations were carried out with the B3LYP[3] exchange-correlation functional including Grimme's D3 dispersion correction[29] and the all-electron double-ζ basis set with polarization function (DZP). COSMO implicit solvation model was used to incorporate the solvation environment (water).

The free energy in the solution-phase G(sol) has been calculated as follows:

$$G(\text{sol}) = G(\text{gas}) + G(\text{solv}) \tag{10}$$

$$G(\text{gas}) = H(\text{gas}) - TS(\text{gas}) \tag{11}$$

$$H(\text{gas}) = E(\text{SCF}) + \text{ZPE} \tag{12}$$

$$\Delta E(\text{SCF}) = \sum E(\text{SCF}) \text{ for products} - \sum E(\text{SCF}) \text{ for reactants} \tag{13}$$

DOI: 10.1021/acs.organomet.8b00456
Organometallics 2018, 37, 3228−3239

$$\Delta G(\text{sol}) = \sum G(\text{sol}) \text{ for products} - \sum G(\text{sol}) \text{ for reactants} \quad (14)$$

G(gas) is the free energy in the gas phase, G(sol) is the free energy of solvation as computed using the continuum solvation model, H(gas) is the enthalpy in the gas phase, T is the absolute temperature (298.15 K), S(gas) is the entropy in the gas phase, E(SCF) is the self-consistent field energy, i.e., raw electronic energy as computed from the SCF procedure, and ZPE is the zero-point energy. Note that by entropy here we refer specifically to the vibrational/rotational/translational entropy of the solute(s); the entropy of the solvent is incorporated implicitly in the continuum solvation model.

■ ASSOCIATED CONTENT

Supporting Information

The Supporting Information is available free of charge on the ACS Publications website at DOI: 10.1021/acs.organomet.8b00456.

Computed energy components, Cartesian coordinates, and vibrational frequencies of all of the DFT-optimized structures (PDF)

■ AUTHOR INFORMATION

Corresponding Author

*E-mail for M.-H.B.: mbaik2805@kaist.ac.kr.

ORCID

Ho Ryu: 0000-0001-8450-991X
Hong Ki Kim: 0000-0002-6115-384X
Seoung-Tae Kim: 0000-0003-4067-9567
Mu-Hyun Baik: 0000-0002-8832-8187

Notes

The authors declare no competing financial interest.

Biography

Mu-Hyun Baik is a Professor of Chemistry at KAIST, the Korea Advanced Institute of Science and Technology, and is an Associate Director of the Institute for Basic Science (IBS), Center for Catalytic Hydrocarbon Functionalizations, that operates within the chemistry department of KAIST. The IBS is the Korean version of the Max Planck Institutes and was initiated in Korea in 2012. Called by friends and colleagues "Mookie", because that is easier to pronounce and that is what his mother called him since he was a baby ("Mook-eeh" is an endeared version of his name in Korean), he grew up in Germany, where his family had moved when he was 10 years old.

After completing his Vordiplom (equivalent to a Bachelor's degree) in 1995 at the University of Düsseldorf, he studied at the University of North Carolina at Chapel Hill, joining the laboratory of Cindy Schauer. Although he had wished to do both experiments and computational work, it was quickly discovered that he was utterly useless in the wet laboratory and he resorted to only focusing on computations. After obtaining a Ph.D. in theoretical inorganic chemistry in 2000, Mookie moved to Columbia University for postdoctoral training with Rich Friesner. Working intensively in collaboration with Ged Parkin and Steve Lippard, he completed his postdoctoral work in 2003 and started his independent career at Indiana University Bloomington.

At IU, Mookie's work focused on discovering reaction mechanisms of organic and organometallic catalyses and he was among the first computational chemists who proposed complete, predictive, and realistic mechanistic cycles for complex catalytic reactions, among them water oxidation, CO_2 reduction, C−C coupling, C−H activation, and many other organometallic reactions. In 2015, he left Indiana reluctantly and with much heartache to take his new position in Korea. In addition to continuing to collaborate with many experimentalists, Mookie is one of the few computational chemists who also carries out experiments themselves and current work focuses on using computational tools to be truly predictive and develop new reactions.

■ ACKNOWLEDGMENTS

We thank the Institute for Basic Science in Korea for financial support (IBS-R10-D1). We thank Deyaa AbuSalim, Manoj Mane, and Joon Heo for helpful discussions and suggestions.

■ REFERENCES

(1) (a) Tantillo, D. J. *Applied Theoretical Organic Chemistry*; World Scientific Publishing Europe: London, 2018. (b) Bachrach, S. M. *Computational Organic Chemistry*; Wiley: Hoboken, NJ, 2014.

(2) Baik, M.-H.; Friesner, R. A. Computing Redox Potentials in Solution: Density Functional Theory as A Tool for Rational Design of Redox Agents. *J. Phys. Chem. A* **2002**, *106*, 7407−7412.

(3) (a) Lee, C.; Yang, W.; Parr, R. G. Development of the Colle-Salvetti correlation-energy formula into a functional of the electron density. *Phys. Rev. B: Condens. Matter Mater. Phys.* **1988**, *37*, 785−789. (b) Becke, A. D. Density-functional thermochemistry. III. The role of exact exchange. *J. Chem. Phys.* **1993**, *98*, 5648−5652.

(4) Zhao, Y.; Truhlar, D. G. The M06 suite of density functionals for main group thermochemistry, thermochemical kinetics, noncovalent interactions, excited states, and transition elements: Two new functionals and systematic testing of four M06-class functionals and 12 other functionals. *Theor. Chem. Acc.* **2008**, *120*, 215−241.

(5) (a) Hay, P. J.; Wadt, W. R. Ab Initio Effective Core Potentials for Molecular Calculations. Potentials for the Transition Metal Atoms Sc to Hg. *J. Chem. Phys.* **1985**, *82*, 270−283. (b) Wadt, W. R.; Hay, P. J. Ab Initio Effective Core Potentials for Molecular Calculations. Potentials for Main Group Elements Na to Bi. *J. Chem. Phys.* **1985**, *82*, 284−298. (c) Hay, P. J.; Wadt, W. R. Ab Initio Effective Core Potentials for Molecular Calculations. Potentials for K to Au Including the Outermost Core Orbitals. *J. Chem. Phys.* **1985**, *82*, 299−310.

(6) Dunning, T. H., Jr. Gaussian Basis Sets for Use in Correlated Molecular Calculations. I. The Atoms Boron through Neon and Hydrogen. *J. Chem. Phys.* **1989**, *90*, 1007−1023.

(7) For reviews of implicit solvation models, see: (a) Roux, B.; Simonson, T. Implicit solvent models. *Biophys. Chem.* **1999**, *78*, 1−20. (b) Tomasi, J.; Mennucci, B.; Cammi, R. Quantum Mechanical Continuum Solvation Models. *Chem. Rev.* **2005**, *105*, 2999−3093. (c) Skyner, R. E.; McDonagh, J. L.; Groom, C. R.; van Mourik, T.; Mitchell, J. B. O. A review of methods for the calculation of solution free energies and the modelling of systems in solution. *Phys. Chem. Chem. Phys.* **2015**, *17*, 6174−6191. For the detailed theoretical background and performance of implicit solvation models that are in widespread use, see: (d) Klamt, A.; Schüürmann, G. COSMO: a New Approach to Dielectric Screening in Solvents with Explicit Expressions for the Screening Energy and its Gradient. *J. Chem. Soc., Perkin Trans. 2* **1993**, 799−805. (e) Marenich, A. V.; Olson, R. M.; Kelly, C. P.; Cramer, C. J.; Truhlar, D. G. Self-Consistent Reaction Field Model for Aqueous and

Nonaqueous Solutions Based on Accurate Polarized Partial Charges. *J. Chem. Theory Comput.* **2007**, *3*, 2011−2033. (f) Takano, Y.; Houk, K. N. Benchmarking the Conductor-like Polarizable Continuum Model (CPCM) for Aqueous Solvation Free Energies of Neutral and Ionic Organic Molecules. *J. Chem. Theory Comput.* **2005**, *1*, 70−77. (g) Marenich, A. V.; Cramer, C. J.; Truhlar, D. G. Universal Solvation Model Based on Solute Electron Density and on a Continuum Model of the Solvent Defined by the Bulk Dielectric Constant and Atomic Surface Tensions. *J. Phys. Chem. B* **2009**, *113*, 6378−6396.

(8) (a) Tetrode, H. Die chemische Konstante der Gase und das elementare Wirkungsquantum. *Ann. Phys. (Berlin, Ger.)* **1912**, *343*, 434−442. (b) Sackur, O. Die universelle Bedeutung des sog. elementaren Wirkungsquantums. *Ann. Phys. (Berlin, Ger.)* **1913**, *345*, 67−86.

(9) Simón, L.; Goodman, J. M. How reliable are DFT transition structures? Comparison of GGA, hybrid-meta-GGA and meta-GGA functionals. *Org. Biomol. Chem.* **2011**, *9*, 689−700.

(10) (a) Marten, B.; Kim, K.; Cortis, C.; Friesner, R. A.; Murphy, R. B.; Ringnalda, M. N.; Sitkoff, D.; Honig, B. New Model for Calculation of Solvation Free Energies: Correction of Self-Consistent Reaction Field Continuum Dielectric Theory for Short-Range Hydrogen-Bonding Effects. *J. Phys. Chem.* **1996**, *100*, 11775−11788. (b) Edinger, S. R.; Cortis, C.; Shenkin, P. S.; Friesner, R. A. Solvation Free Energies of Peptides: Comparison of Approximate Continuum Solvation Models with Accurate Solution of the Poisson−Boltzmann Equation. *J. Phys. Chem. B* **1997**, *101*, 1190−1197. (c) Friedrichs, M.; Zhou, R.; Edinger, S. R.; Friesner, R. A. Poisson−Boltzmann Analytical Gradients for Molecular Modeling Calculations. *J. Phys. Chem. B* **1999**, *103*, 3057−3061.

(11) (a) Paizs, B.; Suhai, S. Comparative Study of BSSE Correction Methods at DFT and MP2 Levels of Theory. *J. Comput. Chem.* **1998**, *19*, 575−584. (b) Mayer, I. Interrelations between the a priori and a posteriori BSSE correction schemes. *Int. J. Quantum Chem.* **2004**, *100*, 559−566. (c) Balabin, R. M. Enthalpy difference between conformations of normal alkanes: Intramolecular basis set superposition error (BSSE) in the case of n-butane and n-hexane. *J. Chem. Phys.* **2008**, *129*, 164101−164105.

(12) Yang, Z.; Yang, S.; Yu, P.; Li, Y.; Doubleday, C.; Park, J.; Patel, A.; Jeon, B.-s.; Russell, W. K.; Liu, H.-w.; Russell, D. H.; Houk, K. N. Influence of water and enzyme SpnF on the dynamics and energetics of the ambimodal [6 + 4]/[4 + 2] cycloaddition. *Proc. Natl. Acad. Sci. U. S. A.* **2018**, *115*, E848−E855.

(13) (a) Vásquez, M.; Némethy, G.; Scheraga, H. A. Conformational Energy Calculations on Polypeptides and Proteins. *Chem. Rev.* **1994**, *94*, 2183−2239. (b) Bolhuis, P. G.; Chandler, D.; Dellago, C.; Geissler, P. L. Transition Path Sampling: Throwing Ropes Over Rough Mountain Passes, in the Dark. *Annu. Rev. Phys. Chem.* **2002**, *53*, 291−318. (c) Christen, M.; Van Gunsteren, W. F. On Searching in, Sampling of, and Dynamically Moving through Conformational Space of Biomolecular Systems: A review. *J. Comput. Chem.* **2008**, *29*, 157−166.

(14) Groom, C. R.; Bruno, I. J.; Lightfoot, M. P.; Ward, S. C. The Cambridge Structural Database. *Acta Crystallogr., Sect. B: Struct. Sci., Cryst. Eng. Mater.* **2016**, *72*, 171−179.

(15) (a) Ribeiro, R. F.; Marenich, A. V.; Cramer, C. J.; Truhlar, D. G. Use of Solution-Phase Vibrational Frequencies in Continuum Models for the Free Energy of Solvation. *J. Phys. Chem. B* **2011**, *115*, 14556−14562. (b) Grimme, S. Supramolecular Binding Thermodynamics by Dispersion-Corrected Density Functional Theory. *Chem. - Eur. J.* **2012**, *18*, 9955−9964. (c) Mammen, M.; Shakhnovich, E. I.; Deutch, J. M.; Whitesides, G. M. Estimating the Entropic Cost of Self-Assembly of Multiparticle Hydrogen-Bonded Aggregates Based on the Cyanuric Acid·Melamine Lattice. *J. Org. Chem.* **1998**, *63*, 3821−3830.

(16) Kim, Y.; Hong, S. Rh(III)-Catalyzed 7-Azaindole Synthesis via C−H Activation/annulative Coupling of Aminopyridines with Alkynes. *Chem. Commun.* **2015**, *51*, 11202−11205.

(17) Eyring, H. The Activated Complex in Chemical Reactions. *J. Chem. Phys.* **1935**, *3*, 107−115.

(18) Adhikari, D.; Nguyen, S. T.; Baik, M.-H. A Computational Study of the Mechanism of the [(salen)Cr + DMAP]-Catalyzed Formation of Cyclic Carbonates from CO_2 and Epoxide. *Chem. Commun.* **2014**, *50*, 2676−2678.

(19) Paddock, R. L.; Nguyen, S. T. Chemical CO_2 Fixation: Cr(III) Salen Complexes as Highly Efficient Catalysts for the Coupling of CO_2 and Epoxides. *J. Am. Chem. Soc.* **2001**, *123*, 11498−11499.

(20) Morse, P. M. Diatomic Molecules According to the Wave Mechanics. II. Vibrational Levels. *Phys. Rev.* **1929**, *34*, 57−64.

(21) Baik, M.-H.; Friesner, R. A.; Lippard, S. J. Theoretical Study on the Stability of N-Glycosyl Bonds: Why Does N7-Platination Not Promote Depurination? *J. Am. Chem. Soc.* **2002**, *124*, 4495−4503.

(22) Parr, R. G.; Yang, W. *Density-Functional Theory of Atoms and Molecules*; Oxford University Press: New York, 1989.

(23) Bochevarov, A. D.; Harder, E.; Hughes, T. F.; Greenwood, J. R.; Braden, D. A.; Philipp, D. M.; Rinaldo, D.; Halls, M. D.; Zhang, J.; Friesner, R. A. Jaguar: A High-Performance Quantum Chemistry Software Program with Strengths in Life and Materials Sciences. *Int. J. Quantum Chem.* **2013**, *113*, 2110−2142.

(24) (a) Slater, J. C. *Quantum Theory of Molecules and Solids*; McGraw-Hill: New York, 1974; Vol. *4* (The Self-Consistent Field for Molecules and Solids). (b) Vosko, S. H.; Wilk, L.; Nusair, M. Accurate spin-dependent electron liquid correlation energies for local spin density calculations: a critical analysis. *Can. J. Phys.* **1980**, *58*, 1200−1211.

(25) Ditchfield, R.; Hehre, W. J.; Pople, J. A. Self-Consistent Molecular-Orbital Methods. IX. An Extended Gaussian-Type Basis for Molecular-Orbital Studies of Organic Molecules. *J. Chem. Phys.* **1971**, *54*, 724−728.

(26) Peng, C.; Schlegel, H. B. Combining Synchronous Transit and Quasi-Newton Methods to Find Transition States. *Isr. J. Chem.* **1993**, *33*, 449−454.

(27) te Velde, G.; Bickelhaupt, F. M.; Baerends, E. J.; Fonseca Guerra, C.; van Gisbergen, S. J. A. Chemistry with ADF. *J. Comput. Chem.* **2001**, *22*, 931−967.

(28) Baerends, E. J.; Ziegler, T.; Atkins, A. J.; Autschbach, J.; Baseggio, O.; Bashford, D.; Bérces, A.; Bickelhaupt, F. M.; Bo, C.; Boerrigter, P. M.; Cavallo, L.; Daul, C.; Chong, D. P.; Chulhai, D. V.; Deng, L.; Dickson, R. M.; Dieterich, J. M.; Ellis, D. E.; van Faassen, M.; Fan, L.; Fischer, T. H.; Fonseca Guerra, C.; Franchini, M.; Ghysels, A.; Giammona, A.; van Gisbergen, S. J. A.; Goez, A.; Götz, A. W.; Groeneveld, J. A.; Gritsenko, O. V.; Grüning, M.; Gusarov, S.; Harris, F. E.; van den Hoek, P.; Hu, Z.; Jacob, C. R.; Jacobsen, H.; Jensen, L.; Joubert, L.; Kaminski, J. W.; van Kessel, G.; König, C.; Kootstra, F.; Kovalenko, A.; Krykunov, M. V.; van Lenthe, E.; McCormack, D. A.; Michalak, A.; Mitoraj, M.; Morton, S. M.; Neugebauer, J.; Nicu, V. P.; Noodleman, L.; Osinga, V. P.; Patchkovskii, S.; Pavanello, M.; Peeples, C. A.; Philipsen, P. H. T.; Post, D.; Pye, C. C.; Ramanantoanina, H.; Ramos, P.; Ravenek, W.; Rodríguez, J. I.; Ros, P.; Rüger, R.; Schipper, P. R. T.; Schlüns, D.; van Schoot, H.; Schreckenbach, G.; Seldenthuis, J. S.; Seth, M.; Snijders, J. G.; Solà, M.; Stener, M.; Swart, M.; Swerhone, D.; Tognetti, V.; te Velde, G.; Vernooijs, P.; Versluis, L.; Visscher, L.; Visser, O.; Wang, F.; Wesolowski, T. A.; van Wezenbeek, E. M.; Wiesenekker, G.; Wolff, S. K.; Woo, T. K.; Yakovlev, A. L. *ADF2017*; SCM, Theoretical Chemistry, Vrije Universiteit: Amsterdam, The Netherlands, 2017.

(29) Grimme, S.; Antony, J.; Ehrlich, S.; Krieg, H. A consistent and accurate ab initio parametrization of density functional dispersion correction (DFT-D) for the 94 elements H-Pu. *J. Chem. Phys.* **2010**, *132*, 154104.

DOI: 10.1021/acs.organomet.8b00456
Organometallics 2018, 37, 3228−3239